




General-relativistic simulations of the formation of a magnetized hybrid star

ANSON KA LONG YIP ¹, PATRICK CHI-KIT CHEONG (張志杰) ^{2,3} AND TJONNIE GUANG FENG LI ^{1,4,5}

¹*Department of Physics, The Chinese University of Hong Kong, Shatin, N.T., Hong Kong*

²*Department of Physics & Astronomy, University of New Hampshire, 9 Library Way, Durham NH 03824, USA*

³*Department of Physics, University of California, Berkeley, Berkeley, CA 94720, USA*

⁴*Institute for Theoretical Physics, KU Leuven, Celestijnenlaan 200D, B-3001 Leuven, Belgium*

⁵*Department of Electrical Engineering (ESAT), KU Leuven, Kasteelpark Arenberg 10, B-3001 Leuven, Belgium*

ABSTRACT

Strongly magnetized neutron stars are popular candidates for producing detectable electromagnetic and gravitational-wave signals. A rapid density increase in a neutron star core could also trigger the phase transition from hadrons to deconfined quarks and form a hybrid star. This formation process could release a considerable amount of energy in the form of gravitational waves and neutrinos. Hence, the formation of a magnetized hybrid star is an interesting scenario for detecting all these signals. These detections may provide essential probes for the magnetic field and composition of such stars. Thus far, a dynamical study of the formation of a magnetized hybrid star has yet to be realized. Here, we investigate the formation dynamics and the properties of a magnetized hybrid star through dynamical simulations. We find that the maximum values of rest-mass density and magnetic field strength increase slightly and these two quantities are coupled in phase during the formation. We then demonstrate that all microscopic and macroscopic quantities of the resulting hybrid star vary dramatically when the maximum magnetic field strength goes beyond a threshold of $\sim 5 \times 10^{17}$ G but they are insensitive to the magnetic field below this threshold. Specifically, the magnetic deformation makes the rest-mass density drop significantly, suppressing the matter fraction in the mixed phase. Therefore, this work provides a solid support for the magnetic effects on a hybrid star, so it is possible to link observational signals from the star to its magnetic field configuration.

1. INTRODUCTION

Neutron stars are natural laboratories for studying physics under extreme conditions, which terrestrial experiments cannot reproduce. On the one hand, the density of a neutron star reaches above the nuclear saturation density $\rho_0 \sim 2.8 \times 10^{14}$ g cm⁻³, at which the canonical atomic structure of matter is disrupted. The detailed microphysics and the concerning equation of state at supra-nuclear densities still remain elusive. Exotic matter, such as deconfined quark matter and hyperons, could exist in this ultradense regime (See e.g. Rezzolla et al. 2018 for a review).

Several studies have long proposed compact stars that are partly or wholly composed of deconfined quark matter (Itoh 1970; Bodmer 1971; Witten 1984). These stars are typically interpreted as the products of the phase transition of the hadrons in the original neutron

stars. In particular, when the density inside a neutron star reaches a threshold, a phase transition converting hadrons into deconfined quarks could happen. If this phase transition only occurs in the stellar core, the resulting star is usually called a ‘hybrid star’. A hybrid star generally has a smaller radius and higher compactness than the progenitor neutron star. Therefore, gravitational potential energy of the order of $\sim 10^{52}$ erg is expected to be released when a hybrid star is formed. Significant portions of the released energy could give rise to the emission of neutrinos and gravitational waves. Detecting these phase transition signals provides evidence of deconfined quark matter. Newly born neutron stars in supernovae and accreting neutron stars in binary systems are possible hosts for such a phase transition (See e.g. Weber 1999; Abdikamalov et al. 2009 for reviews).

On the other hand, neutron stars have the strongest magnetic field found in the Universe. Dipole spin-down models allow for the estimation of the surface magnetic field strength of neutron stars. With the surface field strength \mathcal{B}_s , we can classify neutron stars into millisecond

ond pulsars with $\mathcal{B}_s \sim 10^{8-9}$ G, classical pulsars with $\mathcal{B}_s \sim 10^{11-13}$ G, and magnetars with $\mathcal{B}_s \sim 10^{14-15}$ G. Although there is still no direct observation of the interior magnetic field of neutron stars, virial theorem suggests that it could reach 10^{18-20} G (see e.g. Ferrer et al. 2010, Lai & Shapiro 1991, Fushiki et al. 1989, and Cardall et al. 2001). Furthermore, binary neutron star simulations have demonstrated that the local maximum magnetic field can be amplified up to $\sim 10^{17}$ G during the merger (Price & Rosswog 2006; Kiuchi et al. 2015b,a; Aguilera-Miret et al. 2020).

Highly magnetized neutron stars are promising candidates for explaining some puzzling astronomical phenomena, including soft gamma-ray repeaters and X-ray pulsars (Kouveliotou et al. 1998; Hurley et al. 1999; Mereghetti & Stella 1995; Mereghetti et al. 2000; van Paradijs et al. 1995). Moreover, neutron stars can be deformed by the magnetic field, depending on the geometry of the magnetic field. A purely toroidal field induces prolateness (Kiuchi & Yoshida 2008; Kiuchi et al. 2009; Frieben & Rezzolla 2012), while a purely poloidal field causes oblateness to neutron stars (Bocquet et al. 1995; Konno 2001; Yazadjiev 2012). These magnetic-field-induced distortions make rotating neutron stars possible sources for the emission of detectable continuous gravitational waves (Bonazzola & Gourgoulhon 1996). However, the actual field geometry inside neutron stars is still unknown. Stability analyses of magnetized stars suggest that simple geometries are subjected to instabilities (Tayler 1957, 1973; Markey & Tayler 1973, 1974; Wright 1973). Magnetohydrodynamics simulations propose a mixed configuration of toroidal and poloidal fields as the most favored configuration (Braithwaite & Nordlund 2006; Braithwaite & Spruit 2006; Braithwaite 2009). This configuration is usually referred to as the ‘twisted torus’.

Deconfined quarks and strong magnetic fields are expected to be present inside neutron stars, so studying magnetized hybrid stars is necessary to probe the combined effects of these two features. Previous studies have investigated the properties of magnetized hybrid stars by constructing equilibrium models (e.g. Rabhi et al. 2009; Dexheimer et al. 2012; Isayev 2015; Chatterjee et al. 2015; Franzon et al. 2016b,a; Mariani et al. 2022). In particular, Chatterjee et al. (2015) and Franzon et al. (2016a) have demonstrated that the pure field contribution to the energy–momentum tensor primarily contributes to the macroscopic properties of magnetized hybrid stars. In contrast, the magnetic effects in the equation of state and the field-matter interactions have negligible effects on these properties. Moreover, a magnetic field reduces the central density and prevents the

appearance of quark matter. Dynamics of hybrid star have been studied by numerical simulations (Lin et al. 2006; Abdikamalov et al. 2009; Herzog & Röpke 2011; Prasad & Mallick 2018, 2020). Nonetheless, these studies did not take the magnetic field into account. Since the dynamical stability and the possible observational signal of a magnetized hybrid star could not be thoroughly examined through equilibrium modeling, a dynamical study of this star is still indispensable.

In this work, we numerically study the formation of a magnetized hybrid star through general relativistic magnetohydrodynamics simulations. Specifically, we first construct magnetized neutron star equilibrium models by the open-sourced code XNS (Bucciantini & Del Zanna 2011; Pili et al. 2014, 2015, 2017; Soldateschi et al. 2020) and then dynamically evolve these models using the new general relativistic magnetohydrodynamics code Gmunu (Cheong et al. 2020, 2021, 2022). The details of the initial neutron star models, hybrid star models and evolutions are described in Section 2. Next, the results of the formation process and the properties of the resulting star are presented in Sections 3 and 4 respectively. Finally, we provide the conclusions in Section 5.

2. NUMERICAL METHODS

2.1. Initial neutron star models

We construct the non-rotating magnetized neutron star equilibrium models in axisymmetry by the open-sourced code XNS (Bucciantini & Del Zanna 2011; Pili et al. 2014, 2015, 2017; Soldateschi et al. 2020). These equilibrium models serve as initial data for our simulations.

The initial neutron star models are constructed with a polytropic equation of state,

$$P = K\rho^\gamma, \quad (1)$$

where P is the pressure, ρ is the rest-mass density and we choose a polytropic constant $K = 1.6 \times 10^5 \text{ cm}^5 \text{ g}^{-1} \text{ s}^{-2}$ (which equals to 110 in the unit of $c = G = M_\odot = 1$) and a polytropic index $\gamma = 2$.

We specify the specific internal energy ϵ on the initial time-slice by

$$\epsilon = \frac{K}{\gamma - 1} \rho^{\gamma-1}. \quad (2)$$

We adopt a magnetic polytropic law for the toroidal fields

$$\mathcal{B}_\phi = \alpha^{-1} K_m (\rho h \varpi^2)^m \quad (3)$$

where α is the lapse function, K_m is the toroidal magnetization constant, h is the specific enthalpy, $\varpi^2 = \alpha^2 \psi^4 r^2 \sin^2 \theta$, ψ is the conformal factor, (r, θ) are the

Table 1. Properties of the 9 initial neutron star models constructed by the XNS code. All numerical values are rounded off to two decimal places. ρ_c is the central rest-mass density, M_g is the gravitational mass, r_e is the equatorial radius, and \mathcal{B}_{\max} is the maximum toroidal field strength inside the neutron star. All the models have a fixed baryonic mass $M_0 = 1.68 M_\odot$ and the 8 magnetized models also have the same toroidal magnetization index $m = 1$.

Model	ρ_c ($10^{14} \text{ g cm}^{-3}$)	M_g (M_\odot)	r_e (km)	\mathcal{B}_{\max} (10^{17} G)
REF	8.56	1.55	11.85	0.00
T1K1	8.56	1.55	11.85	3.45×10^{-2}
T1K2	8.56	1.55	11.85	6.89×10^{-2}
T1K3	8.57	1.55	11.85	3.44×10^{-1}
T1K4	8.63	1.55	11.92	1.36
T1K5	8.81	1.56	12.15	2.63
T1K6	9.10	1.58	14.43	5.52
T1K7	8.81	1.59	16.21	6.01
T1K8	8.27	1.60	18.64	6.14

radial and angular coordinates in 2D spherical coordinates, and $m \geq 1$ is the toroidal magnetization index.

In total, 9 models are constructed, where ‘REF’ is the non-magnetized reference model and the remaining 8 neutron star models are magnetized. They are part of the models used in [Leung et al. \(2022\)](#). Because we do not intend to perform a comprehensive study of neutron stars with different masses in this work, all models have a fixed baryonic mass $M_0 = 1.68 M_\odot$, which is within the typical range of neutron star mass. Also, the 8 magnetized models have the same toroidal magnetization index $m = 1$ but different values of toroidal magnetization constant K_m . They are arranged in the order of increasing maximum magnetic field strength \mathcal{B}_{\max} , where the model ‘T1K1’ has the lowest strength, and ‘T1K2’ has the second-lowest strength, so on and so forth. (‘T1’ represents the toroidal magnetization index $m = 1$ and ‘K’ indicates the toroidal magnetization constant K_m). The configuration of these models allows a phase transition that occurs inside the stellar core and facilitates comparison with [Leung et al. \(2022\)](#). Table 1 summarizes the detailed properties of all 9 models.

2.2. Hybrid star models and evolution

The MIT bag model equation of state introduced by [Johnson et al. \(1975\)](#) has been widely used to model quark matter inside compact stars (see e.g. [Weber 1999](#); [Glendenning 2012](#) for a review). The MIT bag model equation of state for massless and non-interacting quarks is given by

$$P_q = \frac{1}{3}(e - 4B), \quad (4)$$

where P_q is the pressure of quark matter, e is the total energy density and B is the bag constant.

For the normal hadronic matter, we adopt an ideal gas type of equation of state for the evolution

$$P_h = (\gamma - 1)\rho e \quad (5)$$

where P_h is the pressure of hadronic matter and γ is kept to be 2.

Either two or three parts constitute the hybrid star formed after the phase transition: (i) a hadronic matter region with a rest-mass density below the lower threshold density ρ_{hm} , (ii) a mixed phase of the deconfined quark matter and hadronic matter for the region with a rest-mass density in between the lower threshold density ρ_{hm} and the upper threshold density ρ_{qm} , and (iii) a region of pure quark matter phase with a rest-mass density beyond ρ_{qm} (this might or might not be present in practice, depending on the maximum density reached). With this picture, the equation of state for hybrid stars is given by

$$P = \begin{cases} P_h & \text{for } \rho < \rho_{\text{hm}}, \\ \alpha_q P_q + (1 - \alpha_q) P_h & \text{for } \rho_{\text{hm}} \leq \rho \leq \rho_{\text{qm}}, \\ P_q & \text{for } \rho_{\text{qm}} < \rho, \end{cases} \quad (6)$$

where

$$\alpha_q = 1 - \left(\frac{\rho_{\text{qm}} - \rho}{\rho_{\text{qm}} - \rho_{\text{hm}}} \right)^\delta \quad (7)$$

is a scale factor to quantify the relative contribution due to hadronic and quark matters to the total pressure in the mixed phase. The exponent δ adjusts the pressure contribution due to quark matter. We set 3 values of $\delta \in \{1, 2, 3\}$ to investigate the dynamical effects of varying quark matter contributions. We choose $\rho_{\text{hm}} = 6.97 \times 10^{14} \text{ g cm}^{-3}$, $\rho_{\text{qm}} = 24.3 \times 10^{14} \text{ g cm}^{-3}$ and $B^{1/4} = 170 \text{ MeV}$. This treatment of phase transition is similar to that of [Abdikamalov et al. \(2009\)](#).

We employ the new general relativistic magnetohydrodynamics code **Gmunu** ([Cheong et al. 2020, 2021, 2022](#)) to evolve the stellar models in dynamical spacetime. **Gmunu** solves the Einstein equations in the conformally flat condition approximation based on the multigrid method.

We perform 2D ideal general-relativistic magnetohydrodynamics simulations in axisymmetry with respect to the z -axis and equatorial symmetry using cylindrical coordinates (R, z) . The computational domain covers $[0, 100]$ for both R and z , with the base grid resolution $N_R \times N_z = 32 \times 32$ and allowing 6 AMR levels (effective resolution = 1024×1024). The refinement criteria of AMR is the same as that in [Cheong et al. \(2021\)](#);

Leung et al. (2022). Our simulations adopt TVDLF approximate Riemann solver (Tóth & Odstrčil 1996), 3rd-order reconstruction method PPM (Colella & Woodward 1984) and 3rd-order accurate SSPRK3 time integrator (Shu & Osher 1988). The region outside the star is filled with an artificial low-density ‘atmosphere’ with rest-mass density $\rho_{\text{atm}} \sim 10^{-10} \rho_c$. Since we are restricted to purely toroidal field models and axisymmetry for the simulations, we do not use any divergence cleaning method.

3. FORMATION DYNAMICS

For each of the 9 equilibrium models, we perform simulations for three times, once for each value of the exponent $\delta \in \{1, 2, 3\}$. Consequently, $9 \times 3 = 27$ simulations are performed in total.

Since all simulations exhibit the same behavior, we take one of them as an example to describe the features of the formation dynamics. Here, we choose the simulation with an initial maximum magnetic field strength $\mathcal{B}_{\text{max}} = 5.52 \times 10^{17}$ G (i.e. Initial model T1K6) and an exponent $\delta = 3$. The exponent $\delta = 3$ corresponds to a more substantial phase transition effect, which favors the demonstration of the formation dynamics. As illustrated by the radial profiles of the rest-mass density $\rho(r)$ (top panel) and the magnetic field strength $\mathcal{B}(r)$ (bottom panel) at $t = 0$ ms (grey solid lines), 10 ms (yellow dash-dotted lines), and 20 ms (red dotted lines) in Fig. 1, the resulting hybrid star has a slightly higher central rest-mass density and maximum magnetic field strength after phase transition. In addition, the magnetic field inside the star becomes more concentrated towards the core with a tiny shift of the maximum magnetic field strength position $r_{\mathcal{B}}$ (dashed lines) to smaller values. Furthermore, new configurations of $\rho(r)$ and $\mathcal{B}(r)$ are obtained at $t = 10$ ms and remain until at least $t = 20$ ms.

Fig. 2 shows the time evolution of the maximum values of the rest-mass density $\rho_{\text{max}}(t)$ (brown solid line) and the magnetic field strength $\mathcal{B}_{\text{max}}(t)$ (dark cyan dash-dotted line) relative to their initial values $\rho_{\text{max}}(0)$ and $\mathcal{B}_{\text{max}}(0)$. The equilibrium values obtained at $t = 20$ ms are plotted with dashed lines. We observe similar damped oscillatory behaviors for both quantities and the star is relaxed into a new equilibrium configuration after the phase transition. As discussed in Abdikamalov et al. (2009), this damping is mainly due to numerical dissipation and shock heating. Importantly, these two quantities are coupled in phase during the formation process. Moreover, after reaching their peak values at $t \sim 0.5$ ms, the oscillation amplitudes decrease by a factor of e^{-1} at $t \sim 6$ ms. This damping explains the

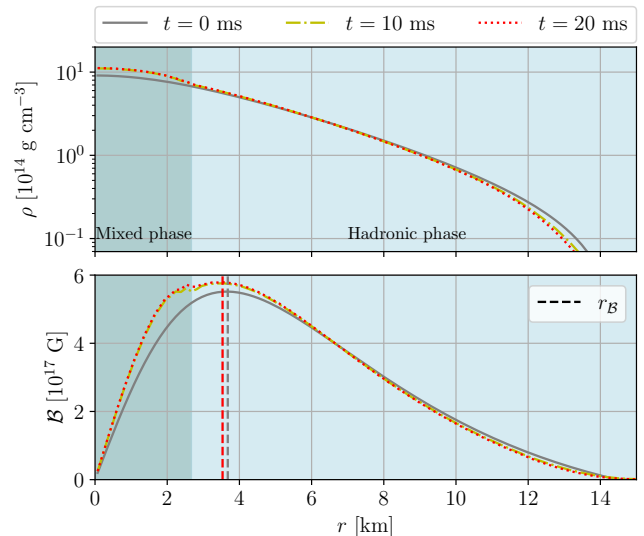


Figure 1. The radial profile of the rest-mass density $\rho(r)$ (top panel) and the magnetic field strength $\mathcal{B}(r)$ (bottom panel) in the equatorial plane for the simulation with the initial model T1K6 and the exponent $\delta = 3$ at $t = 0$ ms (grey solid lines), 10 ms (yellow dash-dotted lines), and 20 ms (red dotted lines). Model T1K6 has an initial maximum magnetic field strength $\mathcal{B}_{\text{max}} = 5.52 \times 10^{17}$ G and δ is an exponent describing the pressure contribution due to quark matter in the mixed phase. The dashed lines in the lower panel represent the maximum magnetic field strength position $r_{\mathcal{B}}$. Cadet blue region represents the portion of the matter in the mixed phase while light blue region denotes the portion of matter in hadronic phase. After phase transition, the resulting hybrid star obtains a slightly higher central rest-mass density and maximum magnetic field strength. Also, the magnetic field inside the star becomes more concentrated towards the core with a tiny shift of $r_{\mathcal{B}}$ to smaller values. Moreover, these new configurations of $\rho(r)$ and $\mathcal{B}(r)$ are obtained at $t = 10$ ms and remain the same until at least $t = 20$ ms.

minor discrepancy between the radial profiles at $t = 10$ ms and $t = 20$ ms as demonstrated in Fig. 1.

4. PROPERTIES OF THE RESULTING MAGNETIZED HYBRID STARS

To better examine the properties of the resulting magnetized hybrid stars, we plot in Fig. 3 different microscopic and macroscopic quantities against the maximum magnetic field strength \mathcal{B}_{max} of the stars. The data points are arranged into 3 sequences with 3 values of $\delta \in \{1, 2, 3\}$, where δ is an exponent quantifying the pressure contribution due to quark matter in the mixed phase. Here, we define the equatorial radius and polar radius of the resulting hybrid stars as the radial positions where the rest-mass density ρ is less than or equal to 10^{-2} of the lower threshold density ρ_{hm} (i.e. $\rho \leq 6.97 \times 10^{12}$ g cm $^{-3}$).

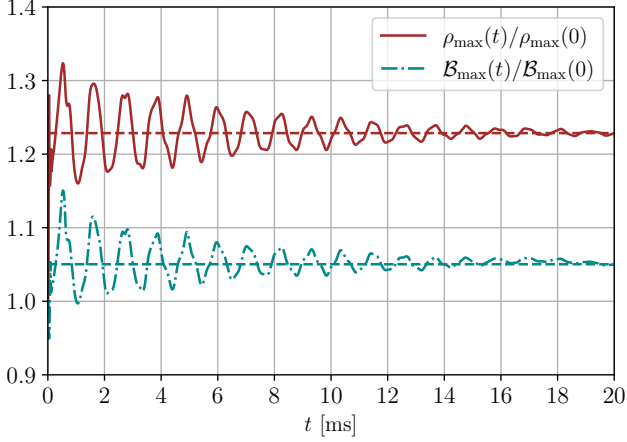


Figure 2. The time evolution of the maximum values of the rest-mass density $\rho_{\max}(t)$ (brown solid line) and the magnetic field strength $\mathcal{B}_{\max}(t)$ (dark cyan dash-dotted line) relative to their initial values $\rho_{\max}(0)$ and $\mathcal{B}_{\max}(0)$ the simulation with the initial model T1K6 and the exponent $\delta = 3$. Model T1K6 has an initial maximum magnetic field strength $\mathcal{B}_{\max} = 5.52 \times 10^{17}$ G and δ is an exponent describing the pressure contribution due to quark matter in the mixed phase. Dashed lines are the equilibrium values of the two quantities obtained at $t = 20$ ms. Similar damped oscillatory behaviors are observed for both quantities and the star is relaxed into a new equilibrium configuration after the phase transition. Importantly, these two quantities are coupled in phase during the formation process. Moreover, after reaching the peak values at $t \sim 0.5$ ms, the oscillation amplitudes are reduced by a factor of e^{-1} at $t \sim 6$ ms.

We find that for $\mathcal{B}_{\max} \gtrsim 5 \times 10^{17}$, all microscopic and macroscopic quantities vary strongly with \mathcal{B}_{\max} , irrespective of δ . When $\mathcal{B}_{\max} \lesssim 3 \times 10^{17}$ G, all quantities vary slightly with \mathcal{B}_{\max} . This means that it may be possible to link observational signals from a magnetized hybrid star to the magnetic field of the star.

Specifically, the central rest-mass density ρ_c (top left panel) and the baryonic mass fraction of the matter in the mixed phase M_{mp}/M_0 (bottom left panel) decrease with \mathcal{B}_{\max} . These decreasing behaviors could be understood in terms of magnetic pressure. As the magnetic pressure becomes more dominant due to the increasing \mathcal{B}_{\max} , matter is pushed off-center to a greater extent. As a result, the rest-mass density ρ in the stellar core reduces, giving a smaller ρ_c . Moreover, as described in Eq. (6), reducing ρ in the core contributes to a smaller fraction of matter that undergoes the phase transition and thus gives a smaller M_{mp}/M_0 .

Moreover, the equatorial radius r_e (top middle panel), the polar radius to equatorial radius ratio r_p/r_e (bottom middle panel) and the gravitational mass M_g (top right panel) all increase with \mathcal{B}_{\max} . The increase in M_g is due to the increasing contribution of the magnetic field

to M_g (corresponds to the increasing \mathcal{B}^2 term of Eq. (B1) in Pili et al. 2014 for example). The other two increasing trends could be interpreted in terms of magnetic deformation. As the matter is pushed off-center by the increasing magnetic pressure, both r_p and r_e increase and the star then deviates from spherical symmetry. Previous studies of magnetized neutron star equilibrium models (e.g. Kiuchi & Yoshida 2008; Kiuchi et al. 2009; Friebe & Rezzolla 2012) indicate that a purely toroidal field deforms the stars to prolate shape, corresponding to $r_p/r_e > 1$. Thus, increasing \mathcal{B}_{\max} of the toroidal field in our models causes the increase in r_p/r_e .

We also examine the effect of pressure contribution due to quark matter δ on different quantities of the hybrid stars. δ has a negligible effect on r_e , r_p/r_e and M_g for all values of \mathcal{B}_{\max} . On the contrary, ρ_c and M_{mp}/M_0 increase substantially with δ for $\mathcal{B}_{\max} \lesssim 3 \times 10^{17}$ G but they become less sensitive to δ for $\mathcal{B}_{\max} \gtrsim 5 \times 10^{17}$ G. These increasing trends could be interpreted in relation to pressure reduction. With the increasing value of δ , the contribution due to quark matter to the total pressure becomes more important and the pressure reduction is enlarged. As a result, this enlarged pressure reduction makes the star collapse to a configuration with a higher ρ_c and M_{mp}/M_0 .

We compare our resulting hybrid stars with Franzon et al. (2016a). The magnetized hybrid star models considered in this study are also in axisymmetry, but the magnetic field is purely poloidal. A poloidal field would make the stars oblate instead of prolate. Also, these models have a different baryonic mass $M_0 = 2.2 M_\odot$. These equilibrium models are constructed by solving the coupled Maxwell–Einstein equations. They also employed a more realistic equation of state with both magnetic and thermal effects taken into account.

We plot the normalized gravitational mass M_g/M_g^* against \mathcal{B}_{\max} (bottom right panel) to compare with the models computed in Franzon et al. (2016a) (Red stars), where M_g^* is the gravitational mass of the non-magnetized reference models. We observe that M_g/M_g^* increases with \mathcal{B}_{\max} similarly for the models in our simulations and Franzon et al. (2016a). Besides, this previous study also found that the magnetic field reduces the central baryon number density and hinders the appearance of matter in quark and mixed phases. These also agree with the trends of ρ_c and M_{mp}/M_0 for our models. Accordingly, despite the disparity in field geometry, baryonic mass, and construction method, our models agree qualitatively with the models in the previous study. This similarity provides additional support that the properties of hybrid the properties of the magnetised hybrid stars presented here are robust.

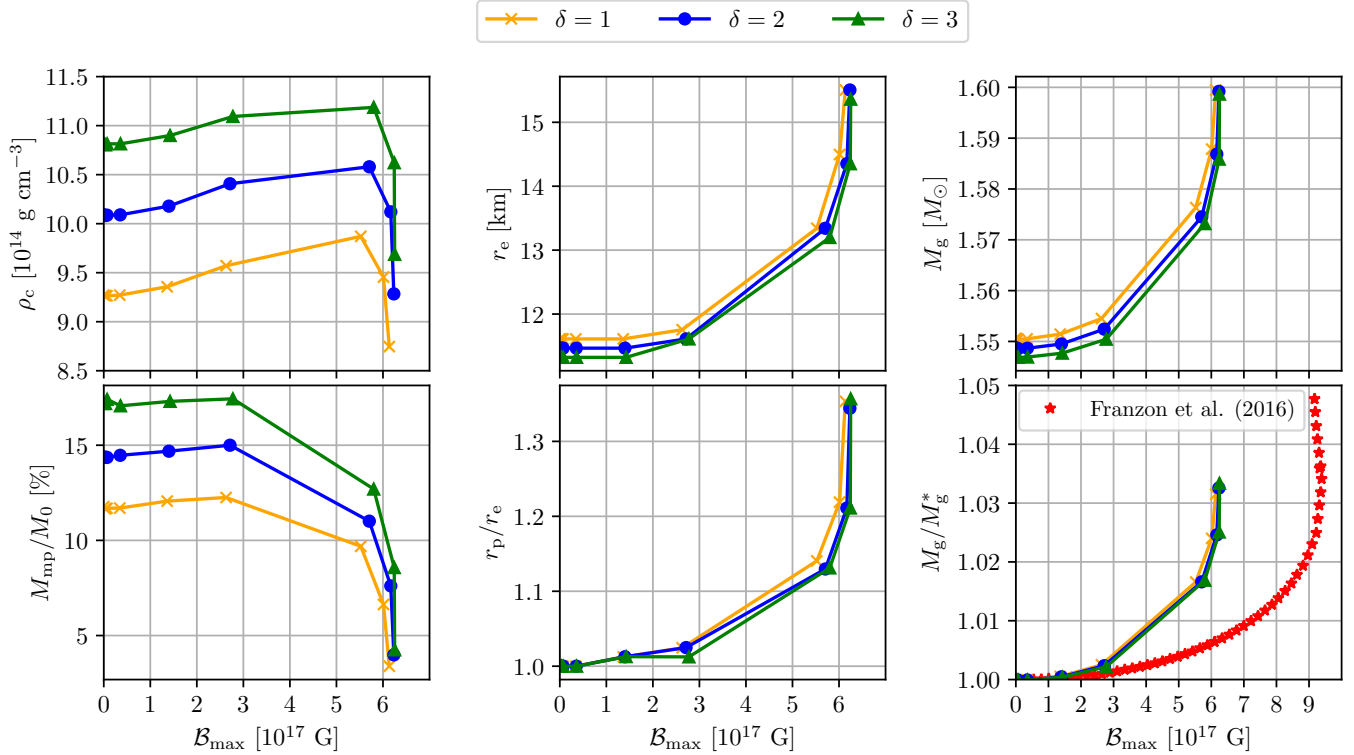


Figure 3. Plots of different microscopic and macroscopic quantities against the maximum magnetic field strength \mathcal{B}_{\max} of our resulting hybrid star models. In particular, we plot the central rest-mass density ρ_c (top left panel), the baryonic mass fraction of the matter in the mixed phase M_{mp}/M_0 (bottom left panel), the equatorial radius r_e (top middle panel), the ratio between polar and the equatorial radii r_p/r_e (bottom middle panel), and the gravitational mass M_g against \mathcal{B}_{\max} (top right panel). The data points are arranged into 3 sequences with 3 values of $\delta \in \{1, 2, 3\}$, where δ is an exponent quantifying the pressure contribution due to quark matter in the mixed phase. The macroscopic and microscopic quantities of all hybrid star models are not sensitive to the magnetic field for $\mathcal{B}_{\max} \lesssim 3 \times 10^{17}$ G. However, these quantities noticeably vary with \mathcal{B}_{\max} for $\mathcal{B}_{\max} \gtrsim 5 \times 10^{17}$ G. In addition, δ has a negligible effect on r_e , r_p/r_e and M_g for all values of \mathcal{B}_{\max} . In contrast, ρ_c and M_{mp}/M_0 increase substantially with δ for $\mathcal{B}_{\max} \lesssim 3 \times 10^{17}$ G but they become less sensitive to δ for $\mathcal{B}_{\max} \gtrsim 5 \times 10^{17}$ G. Furthermore, we plot the normalized gravitational mass M_g/M_g^* against \mathcal{B}_{\max} (bottom right panel) as a comparison with the models computed in Franzone et al. (2016a) (Red stars), where M_g^* is the gravitational mass of the non-magnetized reference models. We find that M_g/M_g^* increases with \mathcal{B}_{\max} similarly for the models in our simulations and Franzone et al. (2016a). Hence, we find agreement amongst vastly different methods and thus provide a solid support for the magnetic effects on a hybrid star.

5. CONCLUSIONS

In this paper, we studied the formation of a magnetized hybrid star by performing 2D axisymmetric general-relativistic magnetohydrodynamics simulations. We first found that the maximum values of rest-mass density and magnetic field strength in the stars rise slightly after a phase transition. The magnetic field also becomes more concentrated towards the center. In addition, the magnetic field and the rest-mass density are coupled during the process. We then investigated the properties of the resulting magnetized hybrid stars. Both macroscopic and microscopic quantities of the hybrid stars are not sensitive to the magnetic field until $\mathcal{B}_{\max} \gtrsim 5 \times 10^{17}$ G, where all quantities change significantly. Specifically, the magnetic deformation decreases the rest-mass density dramatically, leading to a substan-

tial reduction in the matter fraction in the mixed phase. Similar trends for these quantities are found compared with Franzone et al. (2016a).

This work takes the first step to dynamically studying magnetized hybrid stars. Several natural extensions should be considered to model them more realistically. First, a more realistic equation of state, which includes thermal and magnetic effects, should be adopted. In addition, since magnetized stars with purely toroidal fields are expected to be unstable, the suppression of instability in this work is mainly due to the restriction to 2D axisymmetry. The effects of purely poloidal fields and the twisted torus configurations should also be investigated. Since these field geometries extend to the outer region of neutron stars, a force-free/resistive magnetohydrodynamics solver is necessary for more realistic

modeling. Also, 3D simulations without axisymmetry should be conducted to include the instability of magnetic fields. Finally, as most observations suggested that neutron stars rotate, rotations should also be included in future studies.

1 We acknowledge the support of the CUHK Central High-
 2 Performance Computing Cluster, on which the simu-
 3 lations in this work have been performed. This work
 4 was partially supported by grants from the Research
 5 Grants Council of Hong Kong (Project No. CUHK
 6 14306419), the Croucher Innovation Award from the
 7 Croucher Foundation Hong Kong, and the Direct Grant
 8 for Research from the Research Committee of The Chi-
 9 nese University of Hong Kong. P.C.-K.C. acknowl-
 10 edges support from NSF Grant PHY-2020275 (Network
 11 for Neutrinos, Nuclear Astrophysics, and Symmetries
 12 (N3AS)).

Software: XNS (Bucciantini & Del Zanna 2011; Pili et al. 2014, 2015, 2017; Soldateschi et al. 2020), Gmunu (Cheong et al. 2020, 2021, 2022)

REFERENCES

- Abdikamalov, E. B., Dimmelmeier, H., Rezzolla, L., & Miller, J. C. 2009, MNRAS, 392, 52, doi: [10.1111/j.1365-2966.2008.14056.x](https://doi.org/10.1111/j.1365-2966.2008.14056.x)
- Aguilera-Miret, R., Viganò, D., Carrasco, F., Miñano, B., & Palenzuela, C. 2020, PhRvD, 102, 103006, doi: [10.1103/PhysRevD.102.103006](https://doi.org/10.1103/PhysRevD.102.103006)
- Bocquet, M., Bonazzola, S., Gourgoulhon, E., & Novak, J. 1995, A&A, 301, 757, doi: [10.48550/arXiv.gr-qc/9503044](https://doi.org/10.48550/arXiv.gr-qc/9503044)
- Bodmer, A. R. 1971, PhRvD, 4, 1601, doi: [10.1103/PhysRevD.4.1601](https://doi.org/10.1103/PhysRevD.4.1601)
- Bonazzola, S., & Gourgoulhon, E. 1996, A&A, 312, 675, doi: [10.48550/arXiv.astro-ph/9602107](https://doi.org/10.48550/arXiv.astro-ph/9602107)
- Braithwaite, J. 2009, MNRAS, 397, 763, doi: [10.1111/j.1365-2966.2008.14034.x](https://doi.org/10.1111/j.1365-2966.2008.14034.x)
- Braithwaite, J., & Nordlund, Å. 2006, A&A, 450, 1077, doi: [10.1051/0004-6361:20041980](https://doi.org/10.1051/0004-6361:20041980)
- Braithwaite, J., & Spruit, H. C. 2006, A&A, 450, 1097, doi: [10.1051/0004-6361:20041981](https://doi.org/10.1051/0004-6361:20041981)
- Bucciantini, N., & Del Zanna, L. 2011, A&A, 528, A101, doi: [10.1051/0004-6361/201015945](https://doi.org/10.1051/0004-6361/201015945)
- Cardall, C. Y., Prakash, M., & Lattimer, J. M. 2001, ApJ, 554, 322, doi: [10.1086/32137010.48550/arXiv.astro-ph/0011148](https://doi.org/10.1086/32137010.48550/arXiv.astro-ph/0011148)
- Chatterjee, D., Elghozi, T., Novak, J., & Oertel, M. 2015, MNRAS, 447, 3785, doi: [10.1093/mnras/stu2706](https://doi.org/10.1093/mnras/stu2706)
- Cheong, P. C.-K., Lam, A. T.-L., Ng, H. H.-Y., & Li, T. G. F. 2021, MNRAS, 508, 2279, doi: [10.1093/mnras/stab2606](https://doi.org/10.1093/mnras/stab2606)
- Cheong, P. C.-K., Lin, L.-M., & Li, T. G. F. 2020, Classical and Quantum Gravity, 37, 145015, doi: [10.1088/1361-6382/ab8e9c](https://doi.org/10.1088/1361-6382/ab8e9c)
- Cheong, P. C.-K., Pong, D. Y. T., Yip, A. K. L., & Li, T. G. F. 2022, ApJS, 261, 22, doi: [10.3847/1538-4365/ac6cec](https://doi.org/10.3847/1538-4365/ac6cec)
- Colella, P., & Woodward, P. R. 1984, Journal of Computational Physics, 54, 174, doi: [10.1016/0021-9991\(84\)90143-8](https://doi.org/10.1016/0021-9991(84)90143-8)
- Dexheimer, V., Negreiros, R., & Schramm, S. 2012, European Physical Journal A, 48, 189, doi: [10.1140/epja/i2012-12189-y](https://doi.org/10.1140/epja/i2012-12189-y)
- Ferrer, E. J., de La Incera, V., Keith, J. P., Portillo, I., & Springsteen, P. L. 2010, PhRvC, 82, 065802, doi: [10.1103/PhysRevC.82.06580210.48550/arXiv.1009.3521](https://doi.org/10.1103/PhysRevC.82.06580210.48550/arXiv.1009.3521)
- Franzon, B., Dexheimer, V., & Schramm, S. 2016a, MNRAS, 456, 2937, doi: [10.1093/mnras/stv2606](https://doi.org/10.1093/mnras/stv2606)
- Franzon, B., Gomes, R. O., & Schramm, S. 2016b, MNRAS, 463, 571, doi: [10.1093/mnras/stw1967](https://doi.org/10.1093/mnras/stw1967)
- Friebe, J., & Rezzolla, L. 2012, MNRAS, 427, 3406, doi: [10.1111/j.1365-2966.2012.22027.x10.48550/arXiv.1207.4035](https://doi.org/10.1111/j.1365-2966.2012.22027.x10.48550/arXiv.1207.4035)
- Fushiki, I., Gudmundsson, E. H., & Pethick, C. J. 1989, ApJ, 342, 958, doi: [10.1086/167653](https://doi.org/10.1086/167653)
- Glendenning, N. K. 2012, Compact stars: Nuclear physics, particle physics and general relativity (Springer Science & Business Media)
- Herzog, M., & Röpke, F. K. 2011, PhRvD, 84, 083002, doi: [10.1103/PhysRevD.84.083002](https://doi.org/10.1103/PhysRevD.84.083002)
- Hurley, K., Li, P., Kouveliotou, C., et al. 1999, ApJL, 510, L111, doi: [10.1086/311820](https://doi.org/10.1086/311820)
- Isayev, A. A. 2015, in Journal of Physics Conference Series, Vol. 607, Journal of Physics Conference Series, 012013, doi: [10.1088/1742-6596/607/1/012013](https://doi.org/10.1088/1742-6596/607/1/012013)

- Itoh, N. 1970, *Progress of Theoretical Physics*, 44, 291, doi: [10.1143/PTP.44.291](https://doi.org/10.1143/PTP.44.291)
- Johnson, K., et al. 1975, *Acta Phys. Pol. B*, 6, 8
- Kiuchi, K., Cerdá-Durán, P., Kyutoku, K., Sekiguchi, Y., & Shibata, M. 2015a, *PhRvD*, 92, 124034, doi: [10.1103/PhysRevD.92.124034](https://doi.org/10.1103/PhysRevD.92.124034)
- Kiuchi, K., Kotake, K., & Yoshida, S. 2009, *ApJ*, 698, 541, doi: [10.1088/0004-637X/698/1/54110.48550/arXiv.0904.2044](https://doi.org/10.1088/0004-637X/698/1/54110.48550/arXiv.0904.2044)
- Kiuchi, K., Sekiguchi, Y., Kyutoku, K., et al. 2015b, *PhRvD*, 92, 064034, doi: [10.1103/PhysRevD.92.064034](https://doi.org/10.1103/PhysRevD.92.064034)
- Kiuchi, K., & Yoshida, S. 2008, *PhRvD*, 78, 044045, doi: [10.1103/PhysRevD.78.04404510.48550/arXiv.0802.2983](https://doi.org/10.1103/PhysRevD.78.04404510.48550/arXiv.0802.2983)
- Konno, K. 2001, *A&A*, 372, 594, doi: [10.1051/0004-6361:2001055610.48550/arXiv.gr-qc/0105015](https://doi.org/10.1051/0004-6361:2001055610.48550/arXiv.gr-qc/0105015)
- Kouveliotou, C., Dieters, S., Strohmayer, T., et al. 1998, *Nature*, 393, 235, doi: [10.1038/30410](https://doi.org/10.1038/30410)
- Lai, D., & Shapiro, S. L. 1991, *ApJ*, 383, 745, doi: [10.1086/170831](https://doi.org/10.1086/170831)
- Leung, M. Y., Yip, A. K. L., Cheong, P. C.-K., & Li, T. G. F. 2022, *Communications Physics*, 5, 334, doi: [10.1038/s42005-022-01112-w](https://doi.org/10.1038/s42005-022-01112-w)
- Lin, L. M., Cheng, K. S., Chu, M. C., & Suen, W. M. 2006, *ApJ*, 639, 382, doi: [10.1086/499202](https://doi.org/10.1086/499202)
- Mariani, M., Tonetto, L., Rodríguez, M. C., et al. 2022, *MNRAS*, 512, 517, doi: [10.1093/mnras/stac546](https://doi.org/10.1093/mnras/stac546)
- Markey, P., & Tayler, R. J. 1973, *MNRAS*, 163, 77, doi: [10.1093/mnras/163.1.77](https://doi.org/10.1093/mnras/163.1.77)
- . 1974, *MNRAS*, 168, 505, doi: [10.1093/mnras/168.3.505](https://doi.org/10.1093/mnras/168.3.505)
- Mereghetti, S., Cremonesi, D., Feroci, M., & Tavani, M. 2000, *A&A*, 361, 240
- Mereghetti, S., & Stella, L. 1995, *ApJL*, 442, L17, doi: [10.1086/187805](https://doi.org/10.1086/187805)
- Pili, A. G., Bucciantini, N., & Del Zanna, L. 2014, *MNRAS*, 439, 3541, doi: [10.1093/mnras/stu215](https://doi.org/10.1093/mnras/stu215)
- . 2015, *MNRAS*, 447, 2821, doi: [10.1093/mnras/stu2628](https://doi.org/10.1093/mnras/stu2628)
- . 2017, *MNRAS*, 470, 2469, doi: [10.1093/mnras/stx1176](https://doi.org/10.1093/mnras/stx1176)
- Prasad, R., & Mallick, R. 2018, *ApJ*, 859, 57, doi: [10.3847/1538-4357/aabf3b](https://doi.org/10.3847/1538-4357/aabf3b)
- . 2020, *ApJ*, 893, 151, doi: [10.3847/1538-4357/ab7f2b](https://doi.org/10.3847/1538-4357/ab7f2b)
- Price, D. J., & Rosswog, S. 2006, *Science*, 312, 719, doi: [10.1126/science.1125201](https://doi.org/10.1126/science.1125201)
- Rabhi, A., Pais, H., Panda, P. K., & Providência, C. 2009, *Journal of Physics G Nuclear Physics*, 36, 115204, doi: [10.1088/0954-3899/36/11/115204](https://doi.org/10.1088/0954-3899/36/11/115204)
- Rezzolla, L., Pizzochero, P., Jones, D. I., et al. 2018, *Astrophysics and Space Science Library*, Vol. 457, *The Physics and Astrophysics of Neutron Stars* (Springer), doi: [10.1007/978-3-319-97616-7](https://doi.org/10.1007/978-3-319-97616-7)
- Shu, C.-W., & Osher, S. 1988, *Journal of Computational Physics*, 77, 439, doi: [10.1016/0021-9991\(88\)90177-5](https://doi.org/10.1016/0021-9991(88)90177-5)
- Soldateschi, J., Bucciantini, N., & Del Zanna, L. 2020, *A&A*, 640, A44, doi: [10.1051/0004-6361/202037918](https://doi.org/10.1051/0004-6361/202037918)
- Tayler, R. J. 1957, *Proceedings of the Physical Society B*, 70, 31, doi: [10.1088/0370-1301/70/1/306](https://doi.org/10.1088/0370-1301/70/1/306)
- . 1973, *MNRAS*, 161, 365, doi: [10.1093/mnras/161.4.365](https://doi.org/10.1093/mnras/161.4.365)
- Tóth, G., & Odstrčil, D. 1996, *Journal of Computational Physics*, 128, 82, doi: [10.1006/jcph.1996.0197](https://doi.org/10.1006/jcph.1996.0197)
- van Paradijs, J., Taam, R. E., & van den Heuvel, E. P. J. 1995, *A&A*, 299, L41
- Weber, F. 1999, *Journal of Physics G Nuclear Physics*, 25, R195
- Weber, F. 1999, *Journal of Physics G: Nuclear and Particle Physics*, 25, R195
- Witten, E. 1984, *PhRvD*, 30, 272, doi: [10.1103/PhysRevD.30.272](https://doi.org/10.1103/PhysRevD.30.272)
- Wright, G. A. E. 1973, *MNRAS*, 162, 339, doi: [10.1093/mnras/162.4.339](https://doi.org/10.1093/mnras/162.4.339)
- Yazadjiev, S. S. 2012, *PhRvD*, 85, 044030, doi: [10.1103/PhysRevD.85.04403010.48550/arXiv.1111.3536](https://doi.org/10.1103/PhysRevD.85.04403010.48550/arXiv.1111.3536)